AFRL-DE-
TR-2003-1049

A Study of Mid-IR Laser Active Regions

K.J. Malloy

Office of the Vice Provost for Research, MSC 053370
1, The University of New Mexico
Albuquerque, NM 87131-0001

May 2003

Final Report

AIR FORCE RESEARCH LABORATORY
Directed Energy Directorate
3550 Aberdeen Ave SE
AIR FORCE MATERIEL COMMAND
KIRTLAND AIR FORCE BASE, NM 87117-5776

Using Government drawings, specifications, or other data included in this document for any purpose other than Government procurement does not in any way obligate the U.S. Government. The fact that the Government formulated or supplied the drawings, specifications, or other data, does not license the holder or any other person or corporation; or convey any rights or permission to manufacture, use, or sell any patented invention that may relate to them.

This report has been reviewed by the Public Affairs Office and is releasable to the National Technical Information Service (NTIS). At NTIS, it will be available to the general public, including foreign nationals.

If you change your address, wish to be removed from this mailing list, or your organization no longer employs the addressee, please notify AFRL/DELS, 3550 Aberdeen Ave SE, Kirtland AFB, NM 87117-5776.

Do not return copies of this report unless contractual obligations or notice on a specific document requires its return.

This report has been approved for publication.

RON KASPI, DR-III
Project Manager

FOR THE COMMANDER

JEFFREY SALTER, MAJ, USAF
Chief, Tactical Laser Branch

L. BRUCE SIMPSON, SES
Director, Directed Energy Directorate

REPORT DOCUMENTATION PAGE

Form Approved
OMB No. 0704-0188

1. REPORT DATE *(DD-MM-YYYY)*	**2. REPORT TYPE**	**3. DATES COVERED** *(From - To)*
01-May-2003	Final	01 Aug 2000 – 31 Dec 2002

4. TITLE AND SUBTITLE
A Study of Mid-IR Laser Active Regions

5a. CONTRACT NUMBER
F29601-00-C-0173

5b. GRANT NUMBER

5c. PROGRAM ELEMENT NUMBER
62601F

6. AUTHOR(S)
K.J. Malloy

5d. PROJECT NUMBER
3326

5e. TASK NUMBER
LP

5f. WORK UNIT NUMBER
AD

7. PERFORMING ORGANIZATION NAME(S) AND ADDRESS(ES)

Office of the Vice Provost for Research, MSC 053370
1, The University of New Mexico
Albuquerque, NM 87131-0001

8. PERFORMING ORGANIZATION REPORT NUMBER
317411FT

9. SPONSORING / MONITORING AGENCY NAME(S) AND ADDRESS(ES)
Air Force Research Laboratory
Directed Energy Directorate
3550 Aberdeen Ave. SE
Air Force Materiel Command
Kirtland Air Force Base, NM 87117-5776

10. SPONSOR/MONITOR'S ACRONYM(S)

11. SPONSOR/MONITOR'S REPORT NUMBER(S)
AFRL-DE-TR-2003-1049

12. DISTRIBUTION / AVAILABILITY STATEMENT
Approved for Public Release; Distribution is Unlimited.

13. SUPPLEMENTARY NOTES

14. ABSTRACT

We investigated the formation of InAsSb three dimensional growth on GaSb substrates. Experiments were conducted as a function of the As pressure and monolayer coverage. We also explored the band offsets in the $Ga_{1-x}In_xSb$/GaSb heterojunctions as a function of the InSb alloy concentration, x. Experiments consisted of growth of a series of strained quantum wells (QWs) where the alloy concentration, x and thickness, d of the quantum wells were varied. X-ray analysis was used to determine the composition and thickness and to monitor the onset of relaxation. We have grown single quantum wells of strained $Ga_{1-x}In_xSb$ ($x<0.35$) embedded in GaSb by molecular beam epitaxy to investigate the photoluminescence and the band offset of this heterojunction. The photoluminescence shifts to longer wavelengths when the well thickness, or the indium content x, is increased. The band offsets of these heterojunctions are estimated by fitting the photoluminescence data to a single quantum well model. Our offset estimates support the theoretical prediction by first principles calculations for these strained heterojunctions.

15. SUBJECT TERMS
antimonides, InAsSb, band-offsets

16. SECURITY CLASSIFICATION OF:			**17. LIMITATION OF ABSTRACT**	**18. NUMBER OF PAGES**	**19a. NAME OF RESPONSIBLE PERSON**
a. REPORT	**b. ABSTRACT**	**c. THIS PAGE**			Ron Kaspi
UNCLASSIFIED	UNCLASSIFIED	UNCLASSIFIED	UNLIMITED	33	**19b. TELEPHONE NUMBER** *(include area code)* (505) 272-7822

Standard Form 298 (Rev. 8-98)
Prescribed by ANSI Std. 239.18

Table of Contents

List of Figures and Tables

Work commenced on this program with **Error! Bookmark not defined.**, and Kevin Malloy of the University of New Mexico principal individuals involved. Our first goal was the further exploration of what had seemed a promising approach - the growth of InSb quantum dot on GaAs substrates. A previous study had suggested that quantum dot behavior had been observed in earlier samples of InSb on GaSb growths. Our study began by investigating the formation of InAsSb three-dimensional growth on GaSb substrates. Experiments were conducted as a function of the As pressure and monolayer coverage

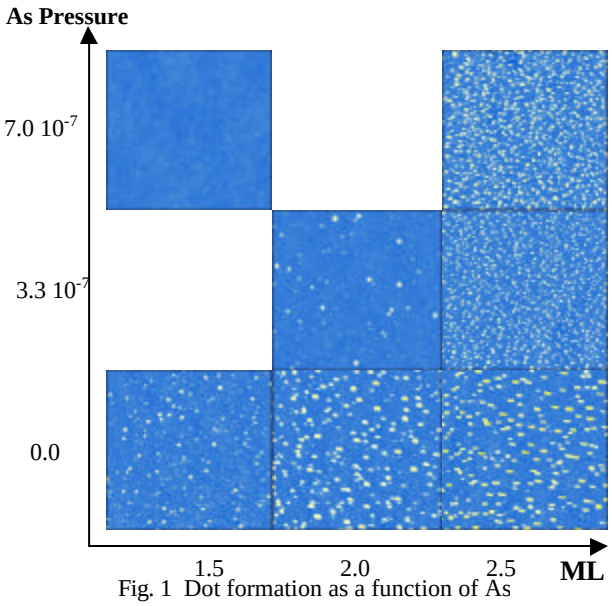

Fig. 1 Dot formation as a function of As pressure and and monolayers deposited

By adjusting the arsenic concentration in the dots it is possible to obtain smaller bandgaps than the parents binary alloys formed by InSb and InAs due to the large bandgap bowing factor of the ternary alloy. Therefore, the resulting quantum dots are expected to show luminescence at even longer wavelength than the InSb quantum dots. In this figure, the trend of dots formation as a function of the Arsenic pressure and the monolayers deposited is shown. Since the arsenic incorporation reduces the strain of the grown material, the reduced dots nucleation while increasing the arsenic partial pressure during the growth indicates the formation quantum dots of the ternary alloy InAsSb. These images were obtained using AFM contact topography. Each image spans 2X2 μm^2.

On the right is the photoluminescence from one of the "dot" samples. The short wavelength peak is the GaSb substrate. While the dot emission may be seen as a strong, slight longer wavelength emission, clearly the behavior of this system is not the same as GaAs/InAs where the dots emit at considerably longer wavelengths than the host.

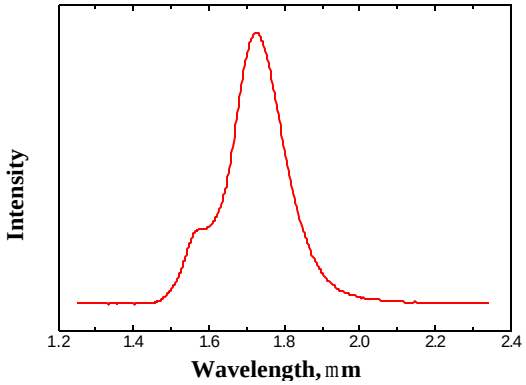

Fig. 2 Photoluminescence spectra from one of the dot samples, showing differing behavior to the GaAs/InAs system

Work continued on this program with **Error! Bookmark not defined.** and Kevin Malloy of the University of New Mexico as the principal individuals involved. Our goal for this quarter was the exploration of the band offsets in the $Ga_{1-x}In_xSb/GaSb$ heterojunctions as a function of the InSb alloy concentration, x. Experiments consisted of growth of a series of strained quantum wells (SQWs) where the alloy concentration, x and thickness, d of the quantum wells were varied. X-ray analysis was used to determine the composition and thickness and to monitor the onset of relaxation. Other samples with quantum dot formation were discussed in previous reports.

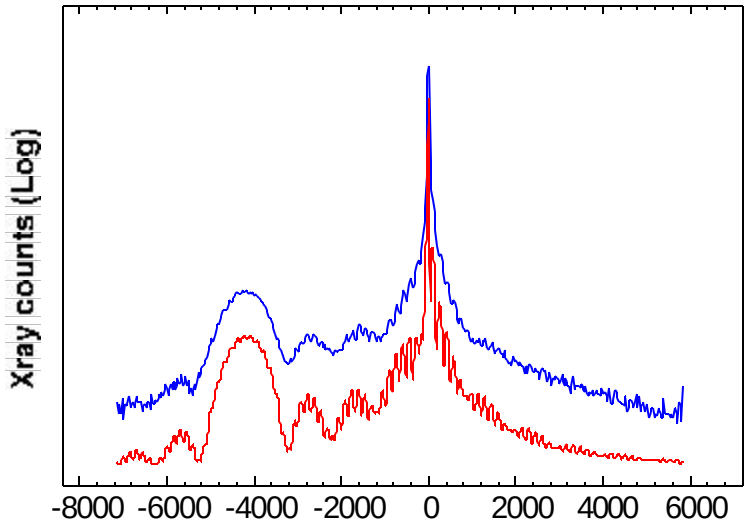

Fig. 3 (004) X ray diffraction for sample 182A

Figure 3 above shows the (004) X ray diffraction for sample 182A. The red line is the best-fit to the measured data (blue line). Based on analysis of the (004) and (115) XRD diffraction, this layer is revealed to be coherently strained with a $Ga_{1-x}In_xSb$ composition of x=30%.

The photoluminescence from the $Ga_{1-x}In_xSb$ strained quantum wells grown by MBE on GaSb was taken with an FTIR while the samples were pumped with an Ar-ion laser. The 10 K photoluminescence spectra from a multiple well sample and a single quantum well sample grown using x=30% $Ga_{1-x}In_xSb$ wells is shown in the next figure. As expected, the emission wavelength increases as a function of either the indium concentration or the well thickness. The solid lines represent the expected luminescence obtained fitting the experimental data to a single band, square well model. As the indium concentration increases, longer wavelengths are accessible. However, larger indium concentrations also increase the strain of the well layer therefore limiting the maximum thickness of the well. These samples do not display any luminescence other than the host GaSb recombination signature.

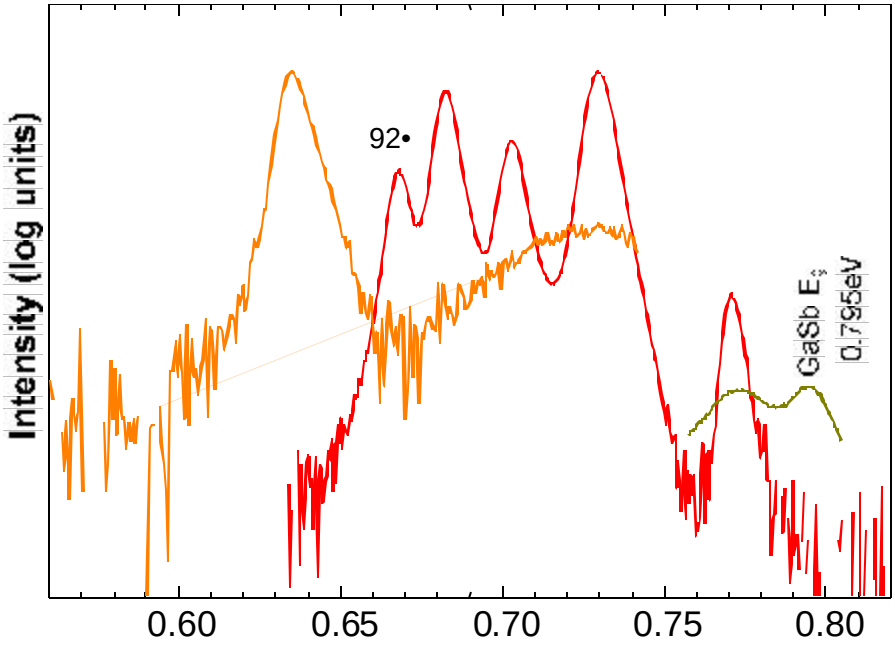

Fig. 4 10K photoluminescence spectra from a multiple well sample and a single quantum well sample grown using x=30% $Ga_{1-x}In_xSb$ wells

Plans for next quarter are continuing this investigation by fitting the data to derive the band offsets in this heterojunction system.

Work continued on this program with **Error! Bookmark not defined.** and Kevin Malloy of the University of New Mexico as the principal individuals involved. Our goal for this quarter was the exploration of the band offsets in the $Ga_{1-x}In_xSb$/GaSb heterojunctions as a function of the InSb alloy concentration, x. Experiments consisted of growth of a series of strained quantum wells (SQWs) where the alloy concentration, x and thickness, d of the quantum wells were varied. X-ray analysis was used to determine the composition and thickness and to monitor the onset of relaxation. Our initial results from photoluminescence and x-ray diffraction were discussed in previous reports.

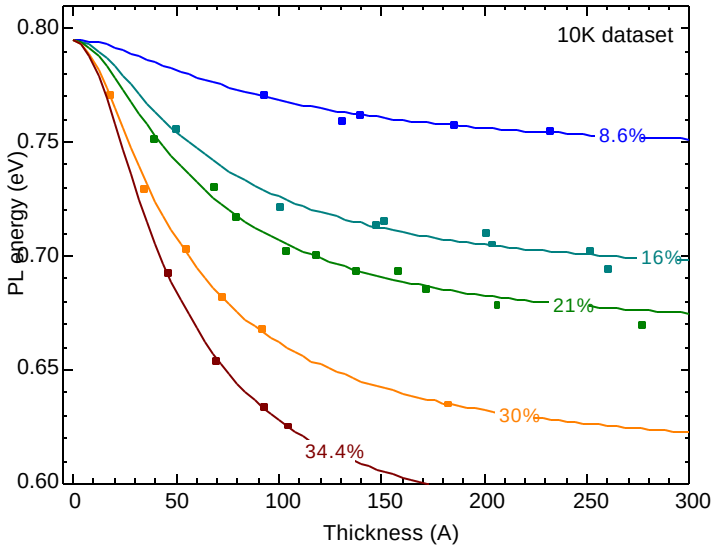

Fig. 5 Photoluminescence energy as a function of well thickness for $Ga_xIn_{1-x}Sb$ strained well on GaSb series

Figure 4 shows the photoluminescence results of our complete series of $Ga_xIn_{1-x}Sb$ strained well on GaSb as a function of the well thickness. The solid lines represent the best fit to the experimental measures obtained by a least square regression.

The experimental data are fit in order to obtain an estimate of the conduction and valence band offsets. We use the single band model in which the valence band and conduction band are treated separately using a single-valued effective mass. Within this single band approximation, the transition energy is given by:

$$E = E_{g,GaSb} - \Delta E_c \, sin^2 \delta_e - \Delta E_{v,hh} \, sin^2 \delta_{hh} ,$$

where $E_{g,GaSb}$ is the energy gap of the GaSb barrier layer, ΔE_c, $\Delta E_{v,hh}$ are respectively the conduction and heavy-holes valence band offsets and δ_e, δ_{hh} are calculated from the following transcendental eigen-energy equation:

$$\sqrt{\frac{2m_{e(hh),well}\Delta E_{c(hh)}}{\eta^2}} L \cos \delta_{e(hh)} = 2atan\left(\sqrt{\frac{m_{e(hh),well}}{m_{e(hh),clad}}} \tan \delta_{e(hh)} \right) + N\pi .$$

Here $m_{e(hh),well}$ is the electron (or heavy hole) mass in the well, L is the thickness and N the order of the solution (N=0 for the ground state).

The effective masses in the GaSb used in this equation are taken from the literature, while the ones in the $Ga_{1-x}In_xSb$ are obtained by linearly interpolating the effective masses of GaSb and InSb. The band offset for the conduction and the heavy-

hole valence band are then used as two independent fitting parameters to the experimental data. The best values for the offset are obtained by least square regression and are reported in table 1 together with their tolerances. Finally, the sensitivity of the band offsets fit as the carrier effective masses are changed was investigated. We found that a change of 50% in the effective masses results in less than 10% change of the offsets values.

Table 1 Least Square and deviation for the band offsets fit. Last entry is from ref. 1.

In	$\Delta E_{v,HH}$	ΔE_c	$E_{c,GaSb}$-ΔE_c	$\sigma_{v,HH}$	σ_c
%	meV	meV	eV	meV	meV
8	21.1	29.2	0.7657	2.0	4.0
16	39.8	65.6	0.7657	0.6	1.2
21	46.0	83.0	0.7119	3.6	3.6
30	63.5	120.0	0.6749	1.2	1.6
35	58.8	160.4	0.6345	1.6	1.6
18	37.0	--	--	--	--

Plans for next quarter are continuing this investigation by comparing the fit data with several theoretical models in the literature.

Work continued on this program with **Error! Bookmark not defined.** and Kevin Malloy of the University of New Mexico as the principal individuals involved. Our investigation of the band offsets in the $Ga_{1-x}In_xSb/GaSb$ heterojunction system as a function of the InSb alloy concentration, x reached a conclusion resulting in the drafting of a paper for publication.

Analysis was performed on experimental results from growth of a series of strained quantum wells (SQWs) where the alloy concentration, x and thickness, d of the quantum wells were varied. Our experimental results from photoluminescence and x-ray diffraction were discussed in previous reports. Our goal for this quarter was a comparison of the experimentally determined offset with theoretically predicted offsets.

In order to compare experiment and theory, the band offsets for the strained $Ga_{1-x}In_xSb$ lattice matched to GaSb must be calculated from the natural (unstrained) band offsets. To do this we make use of the results from the Pikus-Bir Hamiltonian for a strained semiconductor, from which the finite strained well subband energies are given by[1]:

$$V_c = \Delta E_{c0} - a_c(\varepsilon_{xx} + \varepsilon_{yy} + \varepsilon_{zz})$$

for the conduction band discontinuity and by

$$V_{HH} = \Delta E_{v0} - a_v(\varepsilon_{xx} + \varepsilon_{yy} + \varepsilon_{zz}) - \frac{b}{2}(\varepsilon_{xx} + \varepsilon_{yy} - 2\varepsilon_{zz})$$

$$V_{LH} = \Delta E_{v0} - a_v(\varepsilon_{xx} + \varepsilon_{yy} + \varepsilon_{zz}) + \frac{b}{2}(\varepsilon_{xx} + \varepsilon_{yy} - 2\varepsilon_{zz})$$

for the heavy-hole and light-hole valence band discontinuity respectively, In these equations,

$$\varepsilon_{xx} = \varepsilon_{yy} = \frac{a_{GaSb} - a_{InGaSb}}{a_{InGaSb}}$$

$$\varepsilon_{zz} = -2C_{12} / C_{11}\varepsilon_{xx}$$

and ΔE_{v0} is the natural band discontinuity of the heterojunction of the ternary semiconductor given by:

$$\Delta E_{v0}(A_x B_{1-x} C) = xE_{v0,AC} + (1-x)E_{v0,BC}.$$

In order to compare with theory, the theoretical values of Zunger and Wei[2] were taken and the elastic constants and deformation potentials were likewise linearly interpolated. The comparison is summarized in Figure 6 below.

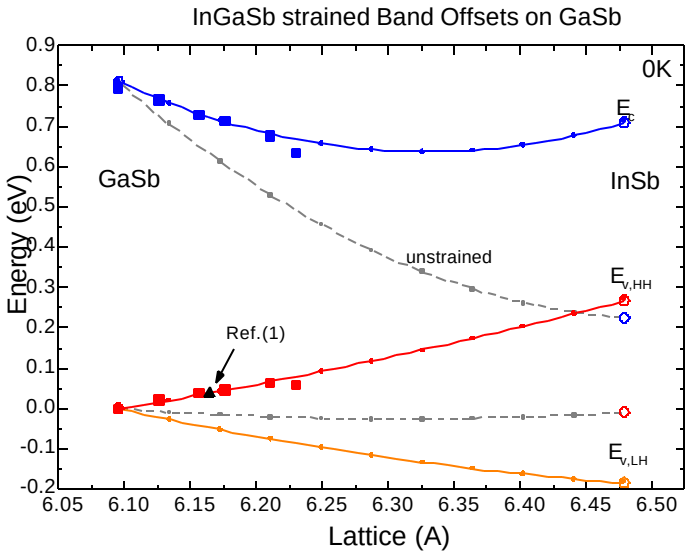

Fig. 6 Comparison of experimental and calculated band offset values

This shows the experimental band offset values obtained from the least square fit of the data (given in quarterly report 5) compared to the calculated band offset of strained $Ga_{1-x}In_xSb$ modeled as described above. Agreement of our experimentally derived offsets with previous studies and with the calculated offset give us confidence that the square well fitting model for strined quantum wells is useful for InSb concentrations up to 30% in the $Ga_{1-x}In_xSb$-on-GaSb heterojunction. At higher In concentrations, however this method becomes less reliable. As strain increases in $Ga_{1-x}In_xSb$, only thinner layers can be grown which generates greater uncertainty in the thickness and composition by XRD measurement. Moreover, since In can diffuse in the barrier layers, the composition profile may differ substantially from an abrupt heterojunction profile on a larger fraction of the well thickness to which this method is very sensitive.

Plans for next quarter are continuing this investigation by comparing the fit data with several other theoretical models in the literature.

Work continued on this program with **Error! Bookmark not defined.** and Kevin Malloy of the University of New Mexico as the principal individuals involved. Our investigation of the band offsets in the $Ga_{1-x}In_xSb/GaSb$ heterojunction system as a function of the InSb alloy concentration, x reached a conclusion resulting in a paper submitted for publication. The final manuscript is attached.

The figure below summarizes one aspect of our findings that was particularly successful. The figure shows the calculated and measured strain shift of the total

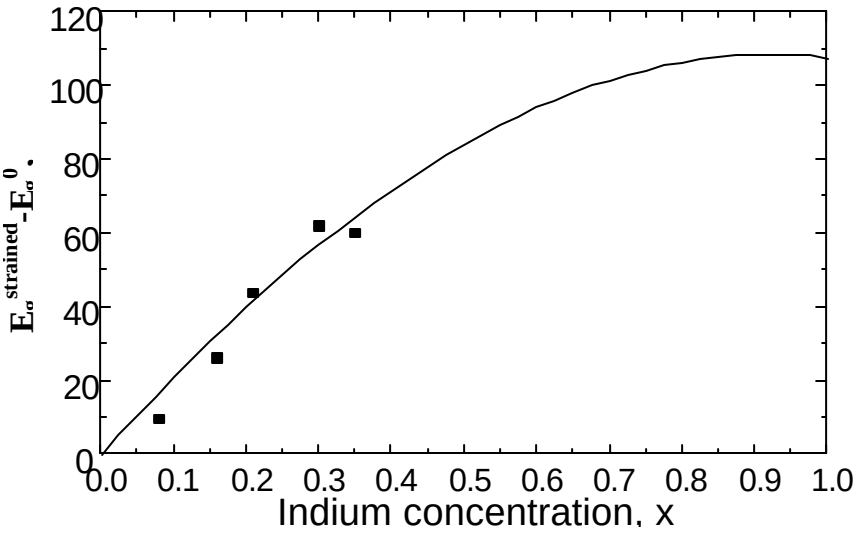

Figure 7. Measured (squares) and calculated (line) variation of $Ga_{1-x}In_xSb$ heavy-hole strained bandgap versus the indium concentration.

bandgap based on the strained quantum well calculations reported previously and referred to in our manuscript. In general, the compressive strain of the $Ga_{1-x}In_xSb$ lattice matched to GaSb increases the bandgap of the $Ga_{1-x}In_xSb$ as shown. The conduction band hydrostatic and the valence band hydrostatic and shear deformation potentials control this effect. The figure emphasizes the consistency between a model using Vegard's law to estimate deformation potentials and elastic constants, and use of a single band model to extract offsets and hence bandgaps from the strained quantum well experiments. This gives us confidence in the reported offsets.

In order to compare experiment and theory, the band offsets for the strained must be calculated from the natural (unstrained) band offsets. To do this we make use of the results from the Pikus-Bir Hamiltonian for a strained semiconductor, from which the finite strained well subband energies are given by[1]:

$$V_c = \Delta E_{c0} - a_c(\varepsilon_{xx} + \varepsilon_{yy} + \varepsilon_{zz})$$

for the conduction band discontinuity and by

$$V_{HH} = \Delta E_{v0} - a_v(\varepsilon_{xx} + \varepsilon_{yy} + \varepsilon_{zz}) - \frac{b}{2}(\varepsilon_{xx} + \varepsilon_{yy} - 2\varepsilon_{zz})$$

$$V_{LH} = \Delta E_{v0} - a_v(\varepsilon_{xx} + \varepsilon_{yy} + \varepsilon_{zz}) + \frac{b}{2}(\varepsilon_{xx} + \varepsilon_{yy} - 2\varepsilon_{zz})$$

for the heavy-hole and light-hole valence band discontinuity respectively, In these equations,

$$\varepsilon_{xx} = \varepsilon_{yy} = \frac{a_{GaSb} - a_{InGaSb}}{a_{InGaSb}}$$

$$\varepsilon_{zz} = -2C_{12}/C_{11}\varepsilon_{xx}$$

and ΔE_{v0} is the natural band discontinuity of the heterojunction of the ternary semiconductor given by:

$$\Delta E_{v0}(A_xB_{1-x}C) = xE_{v0,AC} + (1-x)E_{v0,BC}.$$

In order to compare with theory, the theoretical values of Zunger and Wei[2] were taken and the elastic constants and deformation potentials were likewise linearly interpolated. The comparison is summarized in the next figure.

The figure shows the experimental band offsets values obtained from the least square fit of the data in quarterly report 5 compared to the calculated band offset of strained $Ga_{1-x}In_xSb$ modeled as described above. Agreement of our experimentally derived offsets with previous studies and with the calculated offset give us confidence that the square well fitting model for strined quantum wells is useful for InSb concentrations up to 30% in the $Ga_{1-x}In_xSb$-on-GaSb heterojunction. At higher In concentrations, however this method becomes less reliable. As strain increases in $Ga_{1-x}In_xSb$, only thinner layers can be grown which generates greater uncertainty in the thickness and composition by XRD measurement. Moreover, since In can diffuse in the barrier layers, the composition profile may differ substantially from an abrupt heterojunction profile on a larger fraction of the well thickness to which this method is very sensitive.

Plans for next quarter are continuing this investigation by comparing the fit data with several other theoretical models in the literature.

We have studied the bandgap and band alignment of the semiconductor alloy GaInAsSb. This alloy is technologically important for mid- and far-IR devices. Compositions well inside the miscibility gap of the solid solution were obtained by digital alloy growth techniques and were studied by x-ray diffraction and photoluminescence. Accepted interpolation of the alloy bandgap shows to be inaccurate and a revision is presented. Full details of the study are reported in the appendix.

GaInAsSb lattice matched to GaSb can be conveniently described by $(GaSb)_z(InAs_{0.91}Sb_{0.09})_{1-z}$ where z have a value in the range 0-1. The presence of a miscibility gap however limits the growth of a uniform alloy to composition of $z<0.2$ and $z>0.8$ by use of conventional growth techniques. In the miscibility gap region, different

species tend to segregate into islands of different composition and strain, which in turn enhance even more the segregation processes. This fact is clearly visible when the XRD spectrum of a thin alloy layer is compared to the one of a thick grown layer. To overcome this problem and maintain a uniform composition on thick alloy layers, a digital growth technique can be used. The importance of growing thick layers of GaInAsSb resides in the fact that this material is used as both the absorber material and the wave-guiding core in "W" InAs/GaSb laser structures.
In Fig. 8 we report the bandgap of GaInAsSb samples grown at composition of In=90%, 78.5% 52.5% and 100% (open squares) together with other data obtained from the literature and previous studies (filled squares).

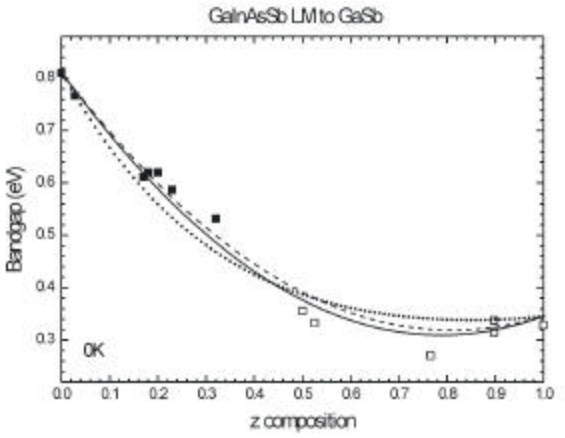

Figure 8 GaInAsSb alloy lattice matched to GaSb, squares are experimental data (open-this study, filled-previous work): lines are the best fits: dashed-Meyer suggested fit, solid-best second order fit to the data, Dots-second order inner matrix product.

The lines represent the best fit. For this alloy Meyer suggested a best second order fit given by:

$$E_g(z)=0.812(1-z)+0.346z-0.75z(1-z) \qquad (1)$$

and is indicated in Fig. 1 with the dashed line. A slight improvement to fit this dataset is obtained, using the same second order equation but with a bowing value of -0.81 eV. The dot line is obtained by using the inner matrix product fit given by:

$$Q(x,y)=\begin{pmatrix} y & y(1-y) & 1-y \end{pmatrix}\cdot\begin{pmatrix} B_1 & C_{12} & B_2 \\ C_{14} & D & C_{23} \\ B_4 & C_{34} & B_3 \end{pmatrix}\cdot\begin{pmatrix} 1-x \\ x(1-x) \\ x \end{pmatrix}, \qquad (2)$$

where the matrix of values is given by:

$$\begin{pmatrix} 0.417 & -0.477 & 1.519 \\ -0.67 & 0.81 & -1.43 \\ 0.235 & -0.415 & 0.812 \end{pmatrix}$$

where the B's and C's were obtained from the literature while D was used as fit parameter.
It is evident from figure 1 that a second order fit is not sufficient to accurately predict the alloy bandgap and that higher orders are necessary. Although it is possible to add a third order to Eq. 1, the fact that some of the data may be quasi-lattice matched to the GaSb substrate, makes questionable the use of a single parameter to characterize the alloy. Equation 2 however, is free from such issues and the third order fit is given by:

$$Q^{(3)}(x,y) = \begin{pmatrix} y & y^2(1-y) & y(1-y)^2 & (1-y) \end{pmatrix} \cdot \begin{pmatrix} B_1 & C_{12} & C_{12} & B_2 \\ C_{14} & D_1 & D_2 & C_{23} \\ C_{14} & D_4 & D_3 & C_{23} \\ B_4 & C_{34} & C_{34} & B_3 \end{pmatrix} \cdot \begin{pmatrix} (1-x) \\ x(1-x)^2 \\ (1-x)x^2 \\ x \end{pmatrix} \quad (3)$$

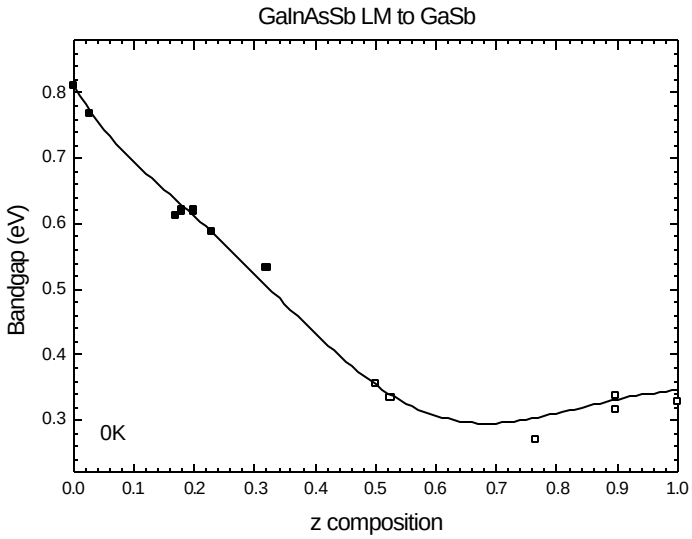

Figure 9 GaInAsSb alloy lattice matched to GaSb, squares are experimental data (open-this study, filled-previous work): the line is the best third order fit from the inner matrix productEq. 3.

where four D coefficients are now needed. Minimization of the error on the data presented gives as a result:

$$D_{ij} = \begin{pmatrix} 0.88 & -5.71 \\ -1.84 & 5.83 \end{pmatrix}$$

The resulting fit is reported in Fig. 9.
Since Eq. 3 is independent of the lattice-matched requirements, it can be used to map the quaternary alloy in the entire compositional space. The result is reported in Fig. 10.

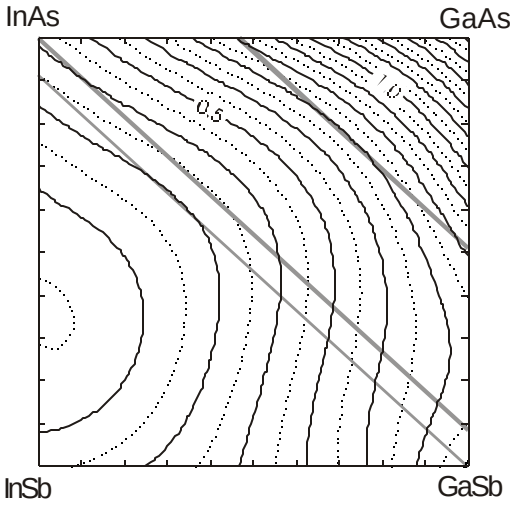

Figure 10 GaInAsSb third order map obtained by using Eq. 3. Straight lines represent the compositions that lattice-match to GaSb, InAs, and InP.

Measurements of valence band offsets were conduced by analysis of the photoluminescence of thin layers versus their thickness. From such analysis, the GaInAsSb alloy lattice matched to GaSb, results to align as type II to GaSb over the whole range of compositions. Two trends are indicative of this situation: the decrease in photoluminescence intensity as the thickness of the wells is increased, which is the opposite trend of a type I alignment and is due to a decrease of the electron hole wave function overlap, and the fact that the emitted wavelength can become longer than the bulk alloy wavelength.

The offsets obtained in this study are reported in Fig. 11. The VBO is measured in reference to the GaSb valence edge and the InAsSb end value here reported is obtained from the literature. In this figure it is evident a strong change in the behavior of the band alignment: for $z<0.75$, the VBO decreases quite linearly while above it, it drastically falls to the lattice matched InAsSb value.

Further studies are in course to fully understand such behavior, however few conclusions addressing W laser structures improvements can be drawn: increasing the indium content of the quaternary absorber used (now about 25%) in order to increase the hole confinement in the W layers, would result in a marginal benefit due to the shallow VBO increase. On the other hand, the reduced bandgap would lower the energy required by the electron to thermalize out of the W layers.

In conclusion, we have reported a detailed study of the technologically important GaInAsSb alloy by mean of digital growth techniques and characterization by XRD and PL spectra.

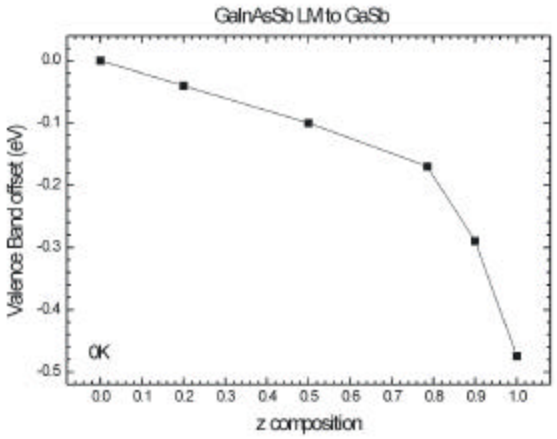

Figure 11 Valence band offset of GaInAsSb lattice-matched to GaSb as obtained by PL single band analysis.

This study showed that a second order interpolation of the alloy lattice matched to GaSb does not accurately describe the bandgap and a revision was proposed. Analysis of the photoluminescence on thin samples indicated two quite different behavior of the valence band alignment with a turn over point close to 75% indium. This result should allow a better understanding of the performances of "W" laser structures.

REFERENCES:

(1) *Optical properties of strained-layer InGaSb/GaSb heterostructures with x<0.4*
L.Q.Qian and B.W.Wessels, J. Vac. Sci. Technol. B 11(4) p. 1652, 1993.

(2) *Physics of optoelectronics devices*
Shun Lien Chuang, Wiley Inter. Science, p.185, 1995

(3) *Calculated natural valence band offsets for all III-V, II-Vi semiconductors*
S.H. Wei and A.Zunger, Phys. Rev. B, 60(8) p. 5404, 1999

APPENDIX:

Estimating the band discontinuity at GaInSb/GaSb heterojunction by investigation of SQW photoluminescence.

G.P.Donati, R.Kaspi, K.Malloy
Center for High Technology Materials, 1313 Goddard St. SE, University of New Mexico, Albuquerque NM 87106 USA

We have grown single quantum wells of strained $Ga_{1-x}In_xSb$ ($x<0.35$) embedded in GaSb by molecular beam epitaxy to investigate the photoluminescence and the band offset of this heterojunction. The photoluminescence shifts to longer wavelengths when the well thickness, or the indium content x, is increased. The band offsets of these heterojunctions are estimated by fitting the photoluminescence data to a single quantum well model. Our offset estimates support the theoretical prediction by first principles calculations for these strained heterojunctions.

As advances in the control of epitaxial growth are made, heterostructures based on III-V antimonides have become strong candidates for mid and far-infrared (>3 μm) opto-electronic device applications[i]. Previous work[i] in these materials has used the compressively strained $Ga_{1-x}In_xSb$ alloy for tailoring optical and electrical characteristics of structures grown on GaSb substrates. Accurate knowledge of electronic parameters, such as bandgap, band offsets and effective masses, is therefore needed. While reliable estimates of bandgap and bowing parameter in this alloy are available in the literature[ii], experimental studies of the band-offsets are limited[iii,iv]. This is partly due to the difficulty of preparing large set of $Ga_{1-x}In_xSb$ samples covering a wide range of compositions.

In this paper, we report a study of the photoluminescence (PL) of strained $Ga_{1-x}In_xSb$ quantum wells (QW) embedded in GaSb, where both the well thickness and the alloy composition, x are systematically varied. The PL spectra show that the emission shifts to longer wavelength upon increasing either the indium concentration or the well thickness. Assuming that the band offset of a fully strained layer is a function only of the alloy composition, the offset is used as the fitting parameter in a finite single band square-well calculation to match the observed PL peak wavelength. In this way, the band discontinuity as a function of x is extracted and compared to theoretical predictions obtained by combining Vegard's law, the natural band alignment[v] and the results of the Pikus-Bir Hamiltonian for strained semiconductors[vi].

Samples were grown by molecular beam epitaxy (MBE). The growth rate and the layer composition were calibrated using RHEED oscillations and subsequently confirmed by x-ray diffraction (XRD). The layers were prepared on 10x10 mm^2 GaSb:Te substrates. After oxide removal, a 200 nm GaSb buffer layer was deposited at 570 C followed by the GaInSb layer at 490 C. The layers were then capped with 100 nm thick GaSb grown at 530 C. Two different sets of samples were grown at each composition: a (~10 nm thick) single QW (SQW) for XRD measurement of composition and thickness and one with several QWs of differing thicknesses for PL measurements. In these last samples, the GaInSb QWs were grown starting from the thickest and ending with the thinnest. Figure A-1 shows the XRD measurement obtained for the x=0.3 alloy SQW together with the best fit obtained by using x and the layer thickness as fitting parameters. The fit, performed using the Takagi-Taupin dynamical diffraction algorithm[vii], gives values of x=0.2968 and thickness of 18.2 nm, close to the RHEED calibration values. Additional XRD measurements taken at the <115> peak show that this layer is not relaxed, consistent with the critical thickness of 27 nm predicted by energy balance model[viii].

The PL spectra are collected at 10K by a Nicolet FTIR system with the samples mounted in a helium-cooled cryostat and optically pumped with an Ar-ion laser (500 mW). Figure A-2 shows the PL spectra of the multiple QW sample at x=0.30 together with that from the SQW used for XRD in Figure A-1. The difference of the relative intensity in the multiple QW PL spectra is unclear, but may be due to competing generation and transport processes. For the multiple well samples, PL peaks are assigned to the ground electron state-heavy hole recombination (E0-HH0) in each layer with the longer wavelength emission originating from thicker wells.

In Fig. A-3, the PL peak energies, $E(L_i)$, of all the samples are plotted versus the well thickness and grouped for wells of the same composition. The solid lines represent

the energy difference obtained from a finite square well model for the E0-HH0 transition. This energy is given by

$$E_{PL,i} = E_{g,GaSb} - \Delta E_c \sin^2 d_{e,i} - \Delta E_{v,hh} \sin^2 d_{hh,i} \quad , \tag{A-1}$$

where $E_{g,GaSb}$ is the energy gap of the GaSb barrier layer, ΔE_c, $\Delta E_{v,hh}$ are respectively the conduction and heavy-hole valence band offsets and $\delta_{e,i}$, $\delta_{hh,i}$ are calculated from the transcendental eigen-energy equation[ix]:

$$\sqrt{\frac{2m_{e(hh),well}\Delta E_{c(hh)}}{\eta^2}} L_i \cos d_{e(hh),i} = 2\text{atan}\left(\sqrt{\frac{m_{e(hh),clad}}{m_{e(hh),well}}} \tan d_{e(hh),i}\right) + Np \ . \tag{A-2}$$

Here, $m_{e(hh),well}$ is the electron (or heavy hole) mass in the well, L_i is the thickness and N the order of the solution (N=0 for the lowest energy state).

In order to extrapolate the band offset, we use the effective masses (heavy holes) for GaSb reported in the literature[ii], while the effective masses for the GaInSb alloys are obtained by linear interpolation of the GaSb and InSb effective masses[ii]. The band offset for the conduction and the heavy-hole valence band are then used as two independent fitting parameters to the experimental values. Since the well and barrier bandgaps and offsets are related by

$$E_{GaSb} = E_{GaInSb} + \Delta E_c + \Delta E_{v,hh}, \tag{A-3}$$

it would be sufficient to use only one band offset in the fit since both bandgaps are known from literature[ii]. However using both offsets allows us to measure independently the GaInSb bandgap and the ratio $\Delta E_{v,hh}/\Delta E_g$. The values for the offset are obtained from a least square regression by numerically maximizing the error function[x]:

$$p = \exp(-\sum_i (E_{PL,i} - E(L_i))^2),$$

The results are reported in Table A-1 together with their standard deviations.

In Fig. A-4 we plot the experimental offsets versus the alloy composition together with the offsets obtained from theoretical calculations. In order to do this, we first determine the valence band alignment for the ternary compound by using Vegard's law applied to the natural valence band alignment of the binary endpoint semiconductors,

$$\Delta E_{v0}(A_x B_{1-x} C) = x E_{v0,AC} + (1-x) E_{v0,BC} \tag{A-4}$$

The binary valence band alignment has been taken from the first principles all-electron band structure model presented by Wei and Zunger[v]. We include the effect of strain by adding the Pikus-Bir strain interaction to the offset obtained by Eq. (A-4). Thus, for a finite-well, the conduction subband energy discontinuity is given by[vi]:

$$\Delta E_c = \Delta E_{c0} - a_c(\varepsilon_{xx} + \varepsilon_{yy} + \varepsilon_{zz}), \tag{A-5}$$

where a_c is the conduction band deformation potential, while the valence subband energy discontinuities are given by:

$$\begin{aligned} \Delta E_{v,hh} &= \Delta E_{v0} - a_v(e_{xx} + e_{yy} + e_{zz}) - \frac{b}{2}(e_{xx} + e_{yy} - 2e_{zz}) \\ \Delta E_{v,lh} &= \Delta E_{v0} - a_v(e_{xx} + e_{yy} + e_{zz}) + \frac{b}{2}(e_{xx} + e_{yy} - 2e_{zz}) \end{aligned} \tag{A-6}$$

for the heavy-hole and light-hole respectively. Here, a_v is the valence band deformation potential while b is the shear deformation term that removes the degeneracy between the

light and heavy holes. Finally the strain tensor components in these equations are given by:

$$e_{xx} = e_{yy} = \frac{a_{GaSb} - a_{GaInSb}}{a_{GaInSb}}$$
$$e_{zz} = -2C_{12} / C_{11} e_{xx} \quad \text{(A-7)}$$

where C_{ij} are the elastic constants of the strained layer, a_{GaSb} is the lattice constant of GaSb and a_{GaInSb} is the lattice constant of the alloy. The values for the deformation potentials and the elastic constants of the binaries are taken from Ref. [ii], and Vegard's law is used to calculate the values for the ternary alloy.

Results from previous studies[iii] (also included in Table A-1) are consistent with our measurements and modeling. The offsets derived from our photoluminescence data agree well with the offsets derived from the first-principles theoretical calculations when combined with the empirical strain Hamiltonian. This suggests that the simple single band, square well model is a good description of this heterojunction system. However, for indium concentrations exceeding 30%, this technique becomes less reliable. As the strain increases in the GaInSb layer, only a few monolayers can be grown before relaxation via dislocation formation takes place and introduces greater uncertainties in the thickness and composition as measured by XRD. Moreover, since the indium from the well can diffuse into the barrier layers, the spatial composition profile may differ substantially from an abrupt profile.

Finally in Fig. A-5 we plot the strain-induced change of the bandgap energy for the $Ga_{1-x}In_xSb$ alloy versus the indium concentration. These data, listed in Table A-2, describe the change in the bandgap due to the valence and conduction band deformation potentials and are obtained by subtracting the two independently determined band offsets from the GaSb bandgap.

Deformation potentials are difficult to measure experimentally and in general are only known for binary compounds. In principle, an accurate measurement of the unstrained valence and conduction band offsets would permit an experimental determination of alloy's deformation potentials by using equations (A-5) and (A-6). The converse is also true – accurate knowledge of the deformation potentials can allow accurate determination of the natural band offsets. Assuming the validity of our approach, our analysis suggests that the natural InSb valence band edge lies at -0.06 ± 0.01 eV relative to the GaSb valence edge, which is 0.05 eV below the value obtained by first principles, all-electron calculation[v].

In conclusion, we have presented an approach to determining the band offsets in a strained alloy system and showed that a single band model with linearly interpolated deformation potentials explains the observed photoluminescence spectra of GaInSb/GaSb strained quantum wells. The deduced offsets were shown to be consistent with theoretical predictions for this alloy system.

Acknowledgments
I would like to thank A. Gray of Zia Laser Inc. for the useful discussions on XRD and simulations.

Figure Captions

A-1 X-ray diffraction on (004) for $Ga_{0.7}In_{0.3}Sb$ 182A thick. The bottom line is the best-fit to the measured data (top line). Based on (004) and (115) XRD diffraction analysis, this layer shows to be coherently strained.

A-2 10K photoluminescence spectra from a multiple well sample and a single quantum well sample grown at 30% indium.

A-3 Photoluminescence of $Ga_{1-x}In_xSb$ strained well on GaSb as a function of the well thickness. The solid lines represent the best fit to the experimental measures obtained by least square regression of equation (A-1) and (A-2). The fit values are collected in Table A-I.

A-4 Band offsets values obtained by the least square regression (solid squares) of the data in figure 3 compared to the band offset of strained GaInSb as modeled from the literature (solid lines). Broken line is the best linear fit to the data, ? $E_V=(0.21\pm0.01)x$. Open circles are the values obtained by authors of ref. 3.

A-5 Measured (squares) and calculated (line) variation of GaInSb heavy-hole strained bandgap versus the indium concentration.

Table A-1
Values of the band offsets and standard deviation (σ) obtained by the least square regression on the data of figure A-3. Last entries are the values reported in ref. 3.

Table A-2
Deformation potential line coefficients for each composition. This line is given by taking the difference of equations (A-6); ? $E_g/?_{xx}=(a_c+a_v)(1-C_{12}/C_{11})+b(1+2\ C_{12}/C_{11})$. Here, ? E_g is the difference of the strained and unstrained bandgaps.

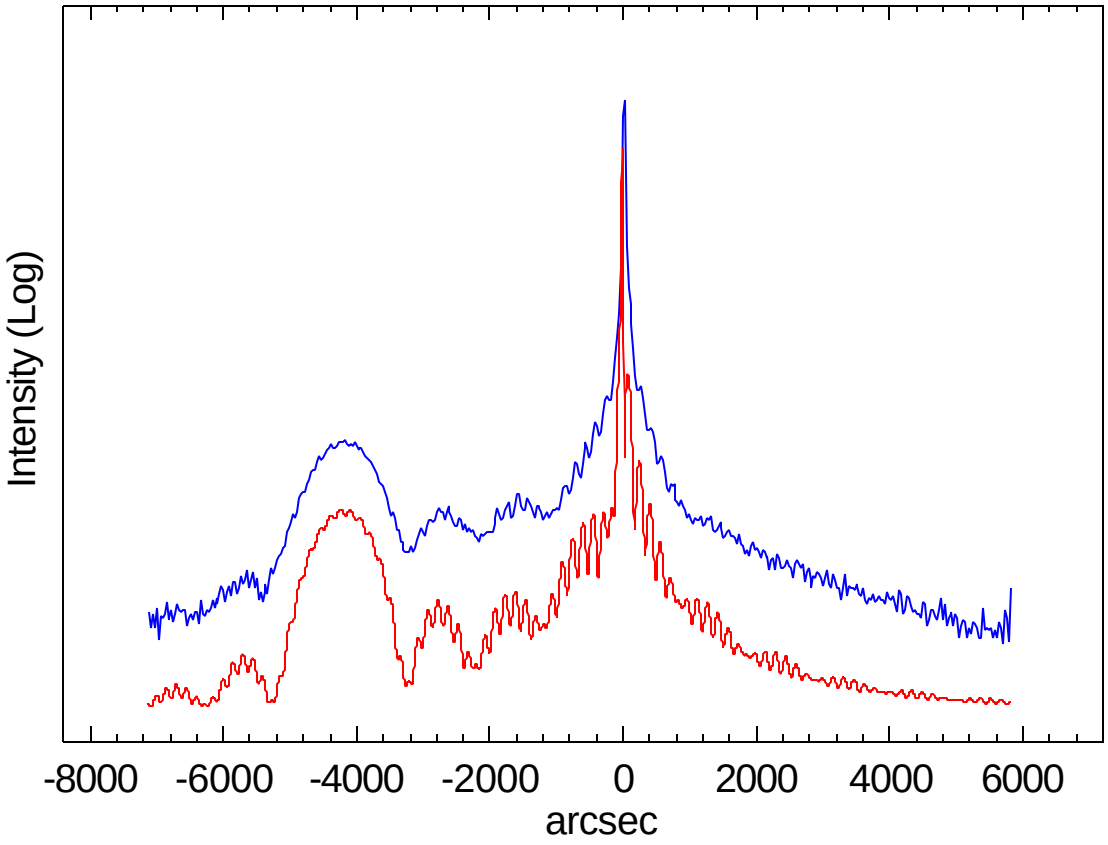
Intensity (Log)
-8000
-6000
-4000
-2000
0
2000
4000
6000
arcsec

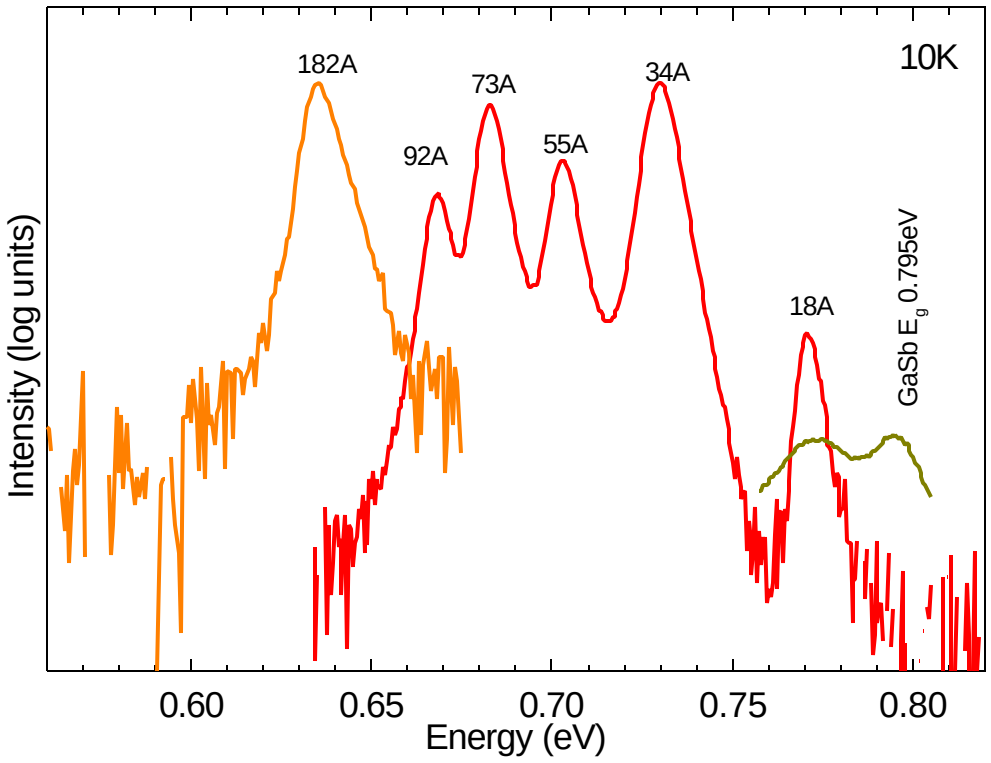
182A
92A
73A
55A
34A
18A
10K
GaSb E_g 0.795eV
Intensity (log units)
0.60
0.65
0.70
0.75
0.80
Energy (eV)

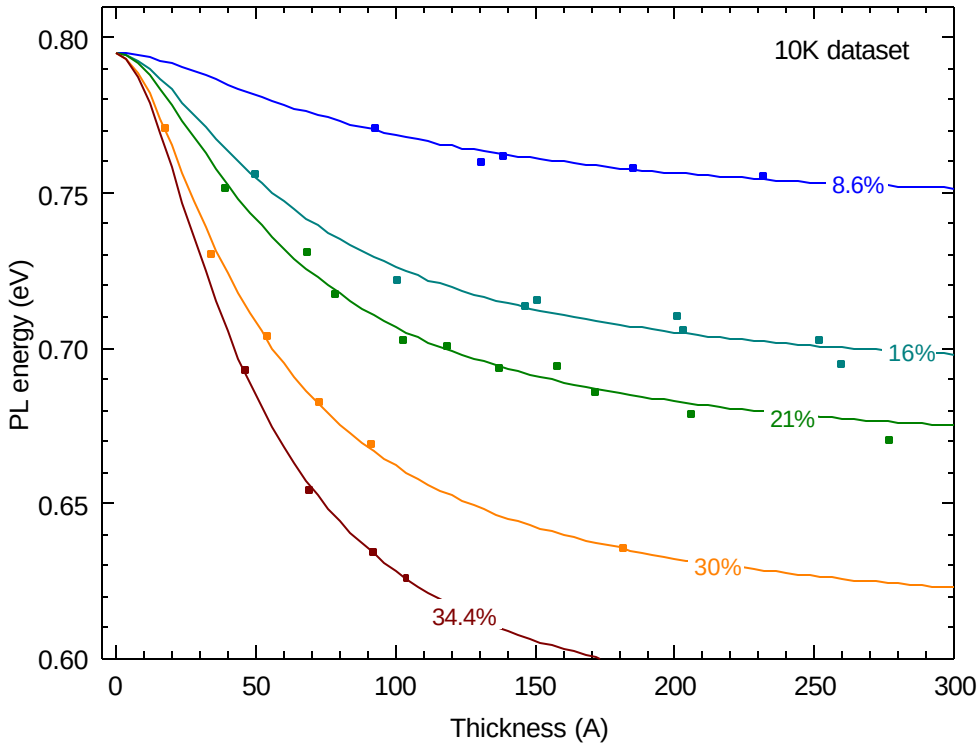

Figure A-3 Donati et *Al*.

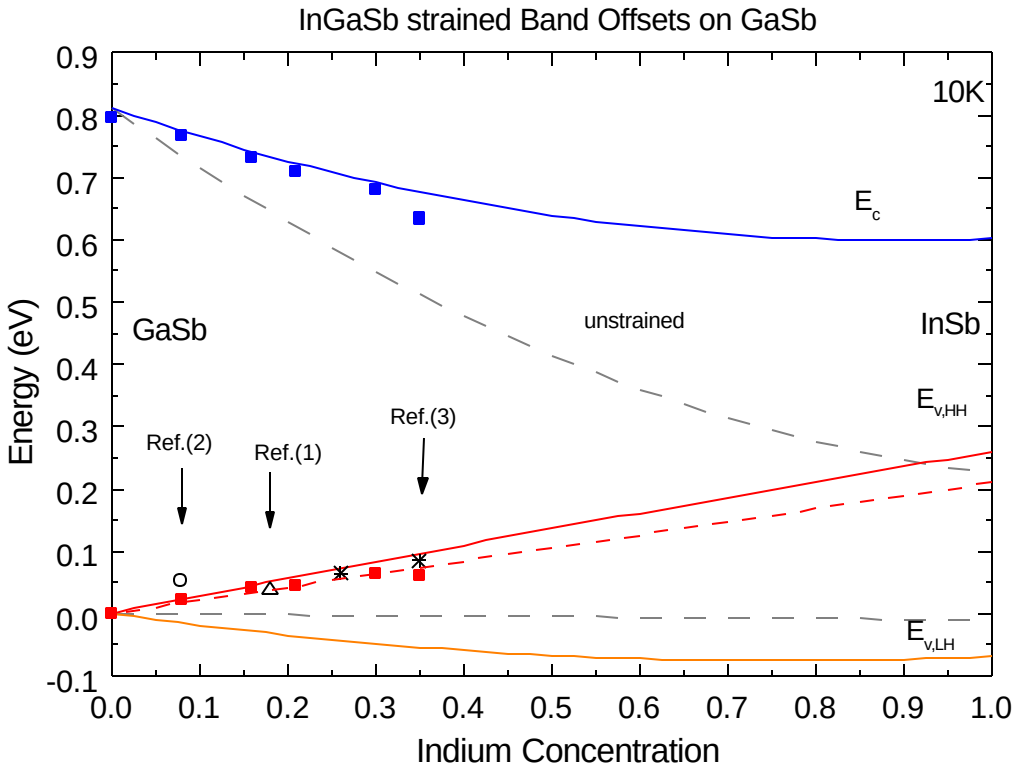
InGaSb strained Band Offsets on GaSb
10K
E_c
$E_{v,HH}$
$E_{v,LH}$
GaSb
InSb
unstrained
Ref.(1)
Ref.(2)
Ref.(3)
Energy (eV)
Indium Concentration
0.9
0.8
0.7
0.6
0.5
0.4
0.3
0.2
0.1
0.0
-0.1
0.0
0.1
0.2
0.3
0.4
0.5
0.6
0.7
0.8
0.9
1.0

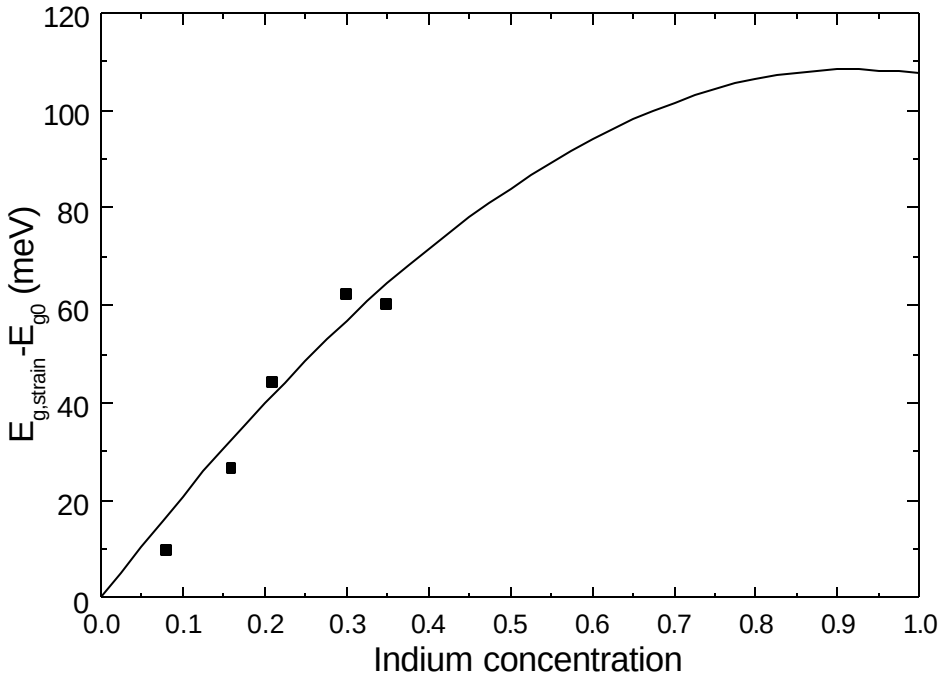
120
100
80
60
40
20
0
0.0
0.1
0.2
0.3
0.4
0.5
0.6
0.7
0.8
0.9
1.0
$E_{g,strain}$-E_{g0} (meV)
Indium concentration

Table A-1 Donati et *Al*.

In %	$\Delta E_{v,HH}$ meV	ΔE_c meV	$E_{c,GaSb}$-ΔE_c eV	$\sigma_{v,HH}$ meV	σ_c meV
8	21.0	29.4	0.766	0.5	0.8
16	40.8	64.3	0.731	3.2	4.2
21	43.4	86.0	0.709	2.4	3.0
30	64.6	116.5	0.678	1.6	1.8
35	59.6	161.5	0.633	1.6	2.0
8	51.6	--	--	--	--
18	37.0	--	--	--	--
26	65	--	--	--	--
35	85	--	--	--	--

In %	$(E_g-E_{g0})/\varepsilon_{xx}$ eV	$1-C_{12}/C_{11}$ []	$1+2C_{12}/C_{11}$ []
8	2.088	0.539	1.922
16	2.704	0.533	1.934
21	3.434	0.529	1.941
30	3.408	0.522	1.956
35	2.751	0.518	1.964

References:

[i] *Type II quantum-well lasers for the mid-wavelength infrared*, J.R.Meyer, C.A.Hoffman, F.J.Bartoli, L.R.Ram-Mohan, Appl.Phys.Lett. **67**(6), 757 (1995)

Midinfrared type-II interband cascade lasers, J.L.Bradshaw, J.D.Bruno, J.T.Pham and D.E.Wortman, R.Q.Yang, J.Vac.Sci.Tech. B, **18**(3), 1628 (2000)

Continuos-Wave Type-II "W" lasers emitting at λ*=5.4-7.1* μ*m,* C.L.Felix, W.W.Bewley, L.J.Olafsen, D.W.Stokes, E.H.Aifer, I.Vurgaftman, J.R.Meyer, M.J.Yang, IEEE Phot. Tech. Lett., **11(**8), 964 (1999)

High power and high brightness from optically pumped InAs/InGaSb type-II mid-IR laser with low confinement, R.Kaspi, A.Ongstad, G.C.Dente, J.Chavez, M.L.Tilton and D.Gianardi, to appear on appl.phys.lett.

High efficiency interband cascade lasers with peak power exceeding 4W/facet, J.L.Bradshaw,R.Q.Yang, J.D.Bruno, J.T.Pham and D.E.Wortman, App.Phys.Lett. **75**(16), 2362 (1999)

[ii] *Band parameters for III-V compound semicond and their alloys*, I.Vurgaftman and J.R.Meyer, J.Appl.Phys. **89**(11), 5815 (2001), and references therein

[iii] *Optical properties of strained-layer InGaSb/GaSb heterostructures with x<0.4*, L.Q.Qian and B.W.Wessels, J. Vac. Sci. Technol. B **11**(4), 1652, 1993

Structural and Optical properties of strained InGaSb/GaSb quantum wells, N.Bertu, R.Klann, A.Mazuelas, O.Brandt, K.H.Ploog and S.Gaillard, App.Phys.Lett. **69**(15), 2237 (1996)

Electroluminescence of GaInSb/GaSb strained single quantum well structures, A.N.Baranov, Y.Cuminal, G.Boissier, J.C. Nicolas, J.L.Lazzari, C.Alibert and A.Joullie', Semicond. Sci.Tech. **11**, 1185 (1996)

[iv] *GaSb/InGaSb strained layer quantum wells by MOCVD,* C.H.Su, Y.K. Su and F.S. Juang, Solid State Electr. **35**(10), 1385 (1992)

[v] *Calculated natural valence band offsets for all III-V, II-VI semiconductors,* S.H. Wei and A.Zunger, Appl.Phys.Lett., **72**(16), 2011 (1998)

[vi] *Physics of optoelectronics devices,* Shun Lien Chuang, Wiley Inter. Science, 185 (1995)

[vii] Takagi-Taupin X-ray scattering equations of dynamical diffraction, Rads Mercury v3.7, Bede Scientific Inc.

[viii] *Calculation of critical thickness versus lattice mismatch,* People and J.C.Bean, Appl.Phys.Lett. **47**(3), 322 (1985)

[ix] *Quantum mechanics,* C.Cohen-Tannoudji, B.Diu, F.Laloe, **1**, 74 (1997)

This transcendental equation follows (for equal particle masses in the clad and the well) from assigning $\delta=atg(k/\alpha)$, where $k=(8\pi^2 mE/h^2)^{1/2}$ and $\alpha=(8\pi^2 m(V-E)/h^2)^{1/2}$ being E the eigen-energy and V the potential offset and using trigonometric relationship. For the case of different particle masses the previous relationship is elliptic and leads to eq. 2.

[x] *An Introduction to error analysis,* J.R.Taylor, University Science Books, 1982

DISTRIBUTION LIST

DTIC/OCP
8725 John J. Kingman Rd, Suite 0944
Ft Belvoir, VA 22060-6218 1 cy

AFRL/VSIL
Kirtland AFB, NM 87117-5776 1 cy

AFRL/VSIH
Kirtland AFB, NM 87117-5776 1 cy

Official Record Copy
AFRL/DELS/R Kaspi 1 cy